inorganics

MDPI

Article

Low-Temperature Fast Firing Preparation of Zn_2TiO_4 Crystalline Photovoltaic Glass Ink and Its Properties

Yongjian Chen, Weixia Dong *, Qifu Bao, Tiangui Zhao, Zhipeng Cheng and Yan Xu

Department of Materials Science and Engineering, Jingdezhen Ceramic University, Xinchang Road, Jingdezhen 333000, China
* Correspondence: 001116@jci.edu.cn

Abstract: A Zn_2TiO_4 crystalline photovoltaic glass ink was prepared by fast firing at 700 °C for 5 min by the glass crystallisation method, which effectively improved the reflectivity and acid resistance of the photovoltaic glass ink coating. The phase, morphology and properties of the samples were tested by XRD, SEM and UV-vis diffuse reflection, etc. The enhanced reflectivity mechanism was proposed. The results showed that the increase in ZnO/SiO_2 ratio reduced the transition temperature (Tg) and crystallisation temperature (Tp) of the glass melt, which could promote the crystallinity of Zn_2TiO_4 in photovoltaic glass ink coatings and thus improve the acid resistance of photovoltaic glass inks. Significant improvement in reflectance and whiteness is due to the Zn_2TiO_4 crystallinity growth, which fills in the pores of the ink surface, and TiO_2 fillers keep almost the same surface roughness (0.2 μm) and wetting angle (5.2°). Typical samples achieved 89.2% of the whiteness and 88.0% of the reflectance, and the weight loss in acid was 3.9 mg/cm^2, which could improve the efficiency of solar power generation.

Keywords: Zn_2TiO_4; photovoltaic glass ink; chemical stability; reflectivity; fast firing

Citation: Chen, Y.; Dong, W.; Bao, Q.; Zhao, T.; Cheng, Z.; Xu, Y. Low-Temperature Fast Firing Preparation of Zn_2TiO_4 Crystalline Photovoltaic Glass Ink and Its Properties. *Inorganics* **2024**, *12*, 169. https://doi.org/10.3390/inorganics12060169

Academic Editors: Kenneth J.D. MacKenzie and Christian Julien

Received: 25 March 2024
Revised: 6 May 2024
Accepted: 27 May 2024
Published: 17 June 2024

1. Introduction

With the increase in environmental pollution and the depletion of natural resources, human beings' demand for clean energy is becoming more and more urgent [1,2]. Photovoltaic materials can convert solar energy into electricity by means of solar cells, so the photovoltaic industry has been developing rapidly [3–5]. Photovoltaic modules consist of cover glass, EVA adhesive, solar cells and back glass. However, the mainstream power generation efficiency of commercially available solar cells is already close to the theoretical value. To improve the power generation efficiency of the solar cells, more efficient cell technology can also be improved through the sunlight and energy density utilization of the module side [6].

Photovoltaic glass ink is composed of ink blending oil, low melting point glass, inorganic filler (rutile TiO_2) and additives, which can be sintered and cured on the double-glass photovoltaic module backplane glass with double-sided power generation technology, as shown in Figure 1. Photovoltaic glass ink coating can reflect the sunlight back to the solar cell and improve the power generation efficiency of the photovoltaic modules [7]. Some literatures have reported that the increase in the coating diffuse reflection is more favourable for improving solar cell utilization [8]. However, the chemical stability of the coating is poor, which shortens the working life. It is well known that the crystal formation in the glass melt can improve the chemical stability and reflection of the coating [9,10]. To our knowledge, there are few reports about crystal formation in photovoltaic glass ink because its quick firing time and low temperature are only 5 min and 700 °C, which is in conflict with the crystal formation time and temperature. Recently, Jiao [9] synthesized $Bi_2Ti_2O_7$ nanocrystals by a glass crystallisation method in 6 min. However, its cost is expensive and the process is complicated. Therefore, seeking a simple, facile and low-cost

method for crystal formation in glass melt is an interesting topic for low-temperature fast firing.

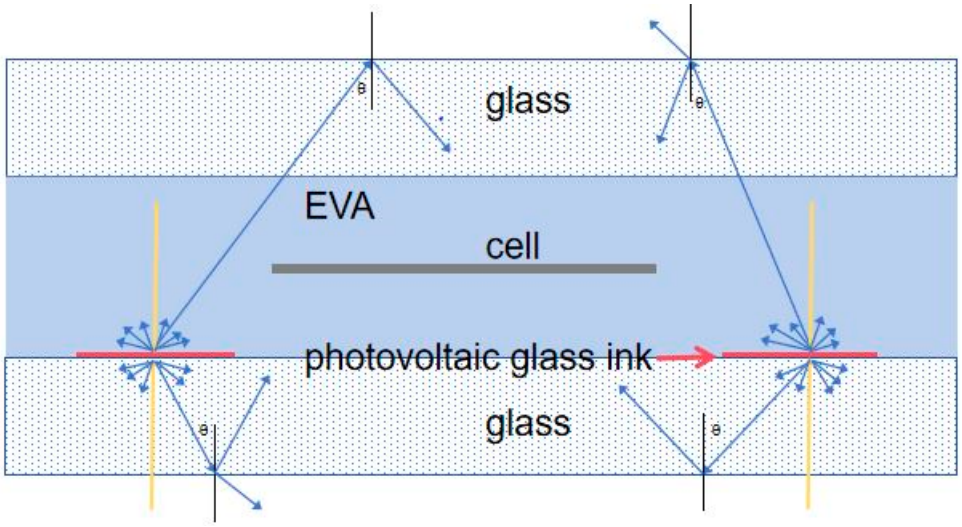

Figure 1. Schematic diagram of the reflection of a photovoltaic glass ink module.

For photovoltaic glass ink, low-melting glass is an important part, which plays a key role in its bonding with the substrate, chemical stability and reflectivity [7,9,11]. Due to its low melting temperature, good thermal stability and electrical insulation, ZnO-B_2O_3-SiO_2 glass systems are often used in glass surface deep processing, glass–metal sealing and other fields [12–15]. However, to our knowledge, there are few reports about ZnO-B_2O_3-SiO_2 glass photovoltaic ink.

In the paper, Zn_2TiO_4 microcrystalline photovoltaic glass ink coating was prepared by changing ZnO/SiO_2 (i.e., ZnO increases and SiO_2 content decreases) fast firing at 700 °C in 5 min, and effects of different ZnO/SiO_2 on the performance of the samples was explored.

2. Experimentation

2.1. Preparation of ZnO-B_2O_3-SiO_2 Low-Melting Glass

All ingredients are pure chemical ingredients from Sinopharm Chemical Reagent Co., Ltd., Shanghai, China. In this experiment, keeping the molar percentages of ZnO and SiO_2 unchanged, the chemical composition consists of 4 mol% Na_2O, 2 mol% K_2O, 5 mol% CaO, 3 mol%, BaO, 30–50 mol% ZnO, 17 mol% B_2O_3, 36–16 mol% SiO_2, 1 mol% Al_2O_3, and 1 mol% TiO_2, with 1 mol% ZrO_2 as nucleating agent. The samples were prepared by changing ZnO/SiO_2 ratios of 30/36, 35/31, 40/26, 45/21 50/16, respectively. The low-melting glass preparation process is shown in Figure 2. The raw materials were weighed and mixed according to the formula, loaded into corundum crucible, placed in a silicon–carbon rod electric furnace and heated up to 1300 °C; the glass liquid was poured into the preheated graphite moulds for the forming and water quenching in cold water; and then the graphite moulds were put into the annealing furnace at 450 °C for 1 h and then cooled naturally. The glass slag obtained from water quenching was ball-milled and crushed through a 200-mesh sieve to obtain ZnO-B_2O_3-SiO_2 low-melting glass (named as low-melting glass).

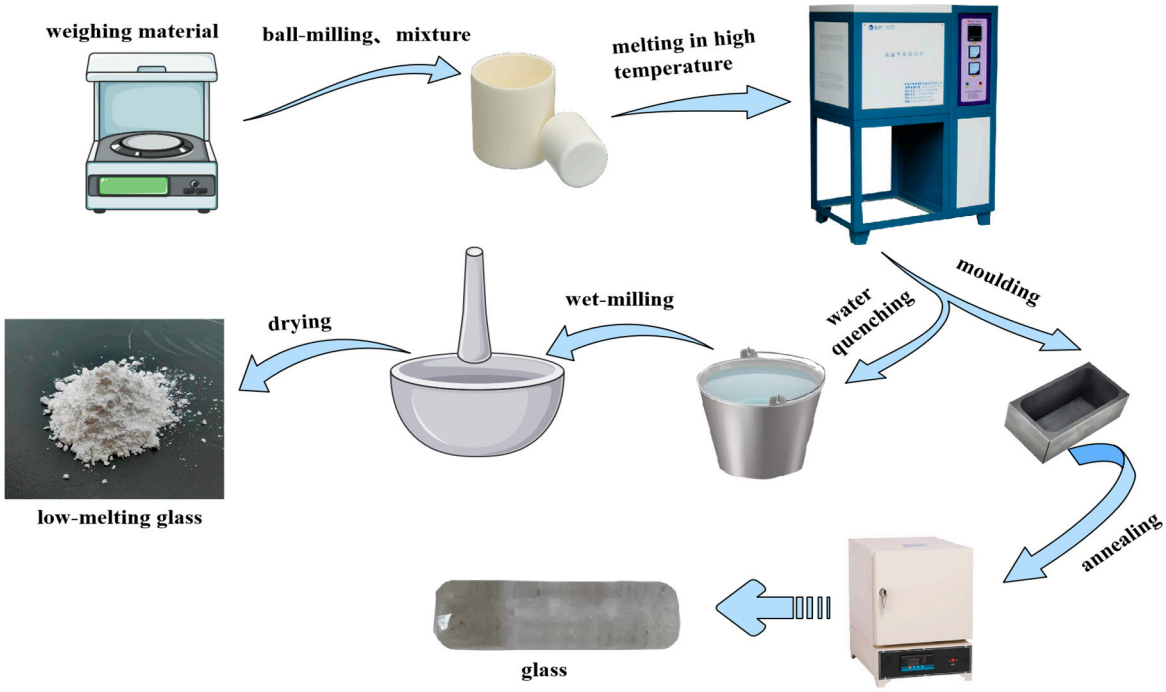

Figure 2. Preparation process diagram of low-melting glass.

2.2. Preparation of the Photovoltaic Glass Ink

The photovoltaic glass ink samples are composed of low-melting glass (75 μm), the ink and TiO_2 (rutile, 200–300 nm). The low-melting glass/TiO_2 quality ratio was 6:4, and the concentration of ink was 30%. The raw materials were mixed, ground in an agate mortar for 20 min, printed on the glass substrate through 160 mesh screen printing (96 μm), and then dried at 110 °C for 15 min. The as-prepared photovoltaic glass ink samples are calcined at 700 °C for 5 min.

2.3. Characterisation

The crystalline phase composition of the samples was observed by XRD (Bruker D8 advance, Karlsruhe, Germany) (CuKα as a ray source, λ = 1.5418 Å, operating voltage 40 V; operating current 30 A, scanning frequency 5°/min, angle 2θ = 5–80°). The microstructure of the samples was characterised by SEM (JSM-6700F, JEOL, Tokyo, Japan) and KYKY-EM3900M (KYKY Technology Co., Ltd, Beijing, China). The chemical composition powder chemical composition was also measured by an EDS system (15 kV) equipped with FESEM equipment (JSM-6700F). Acquisition of 3D surface contours and calculation of surface roughness was performed using the VHX-7000 digital microscope (KEYENCE, Osaka, Japan). Differential thermal tests (DTA) were performed on the glass melts to explore the changes in Tg and Tp. Acid resistance of the photovoltaic glass inks was tested with 10% concentration of citric acid. Whiteness and reflectance of photovoltaic glass inks were determined using a whiteness meter and UV-Vis diffuse reflectance test. The hydrophilicity of the samples was tested by a contact angle meter (JGW-360D, Chengde Chenghui Testing Machine Co., Ltd, Chengde, China).

3. Results and Discussion

3.1. XRD Patterns of Low-Melting Glass

Figure 3 shows XRD patterns of low-melting glass samples prepared with the different ZnO/SiO_2 (i.e., ZnO increases and SiO_2 content decreases). It can be seen that the diffraction peaks of all the samples show bun peaks, and there are no obvious crystalline peaks, indicating that the samples belong to the amorphous phase. The increase in ZnO content in the samples did not result in significant devitrification of low-melting glass.

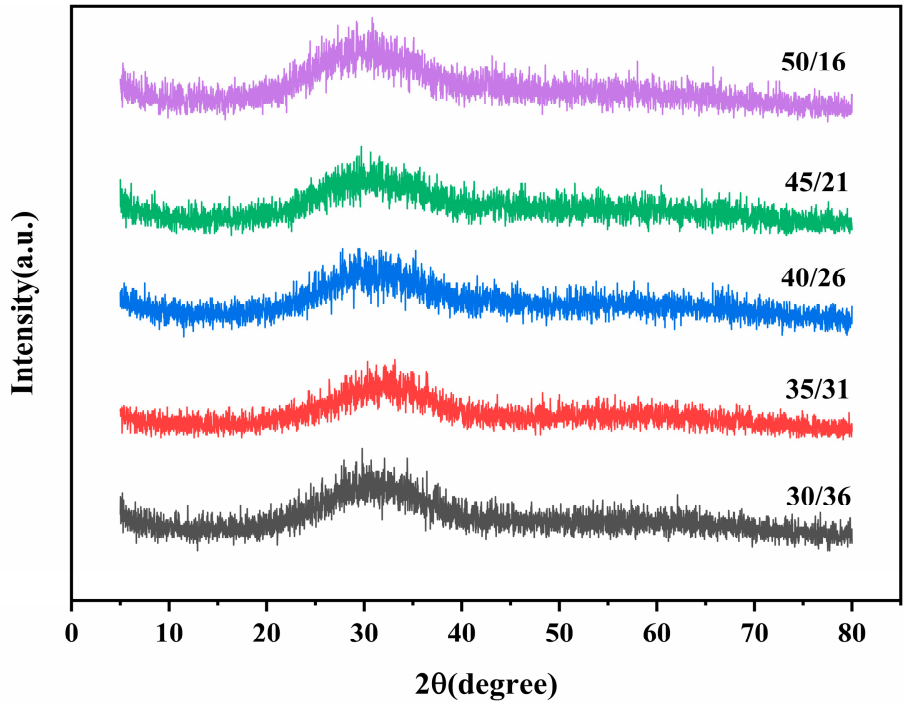

Figure 3. XRD patterns of low-melting glass samples prepared by changing ZnO/SiO_2 ratios.

3.2. DTA Curves of the Glass Melt

Figure 4 shows DTA curves of low-melting glass samples. With the increase in ZnO/SiO_2 (i.e., ZnO increases and SiO_2 content decreases), the transition temperature (Tg) values of low-melting glass samples are 545 °C, 539 °C, 527 °C, 515 °C, and 510 °C, respectively. The devitrification temperature (Tp) also shows a decreasing trend. It can be seen that from the thermal expansion curves of the samples prepared with ZnO/SiO_2 (i.e., ZnO increases and SiO_2 content decreases), with the increase in ZnO/SiO_2 ratio, the melting temperature (T_f) and the transition temperature (T_g) of the samples decrease (Figures 4 and S1), which indicates that increase in ZnO/SiO_2 can lower the melting temperature. As the ZnO/SiO_2 ratio increases from 30/36 to 45/21, the crystallisation peak (Tp) becomes more and more obvious, which is due to the increase in ZnO, the decrease in SiO_2 content, the increase in $[ZnO_4]$ in the melt and the decrease in $[SiO_4]$ (Figure S2), resulting in a decrease in viscosity, where free ions are easier to aggregate, so the crystallisation peak becomes more obvious. However, further increasing the ZnO/SiO_2 ratio to 50/16, T_p of the sample becomes relatively insignificant, which may be due to the precipitation of crystals in the process of melting and cooling of the low-melting glass, resulting in the crystallisation peak of the sample not being obvious in the differential thermal test. However, there is no obvious disintegration peak in the XRD diffraction pattern, which is due to the small crystal size [16,17]. As is known, differential thermal analysis is a process in which the thermal effect is converted into a temperature difference signal and reflected in the differential thermal curve, so differential thermal analysis can indicate the crystallisation of the glass [18,19].

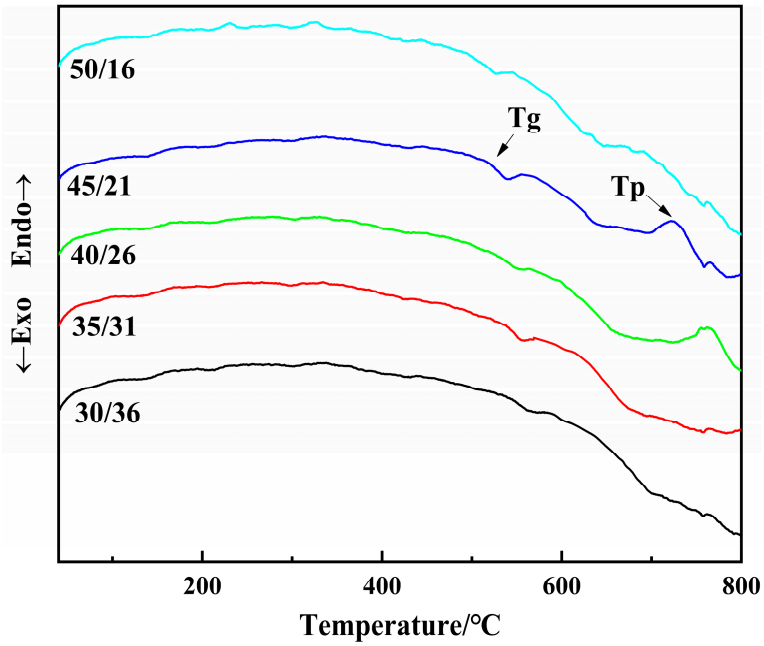

Figure 4. DTA curves of low-melting glass samples prepared by changing ZnO/SiO_2 ratios.

3.3. XRD Patterns

The glass ink was prepared by mixing the low-melting glass with ink mixing oil and was kept at 700°C for 5 min to observe its crystallisation. XRD patterns of the glass ink after sintering samples are shown in Figure 5. 30/36 and 35/31 did not show precipitation peaks, indicating the amorphous glass phases. With the increase in ZnO/SiO_2 (i.e., ZnO increases and SiO_2 content decreases), 40/26 and 45/21 show the diffraction peaks of $Zn_{1.7}SiO_4$ crystals, However, the diffraction patterns of c and d do not show obvious regular changes, which may be the reason for the crystal growth orientation or further research. ZnO as alkaline earth metal oxide can act as the intermediate oxide in the glass network structure; a small amount of ZnO addition results in the formation of $[ZnO_6]$ present outside the glass network, and as the ZnO content increases, the $[ZnO_4]$ content in the glass increases and enters the glass network structure [9]. Further increasing the ZnO/SiO_2 ratio, the sharp diffraction peaks of ZnO appeared in 50/16 due to too much ZnO content.

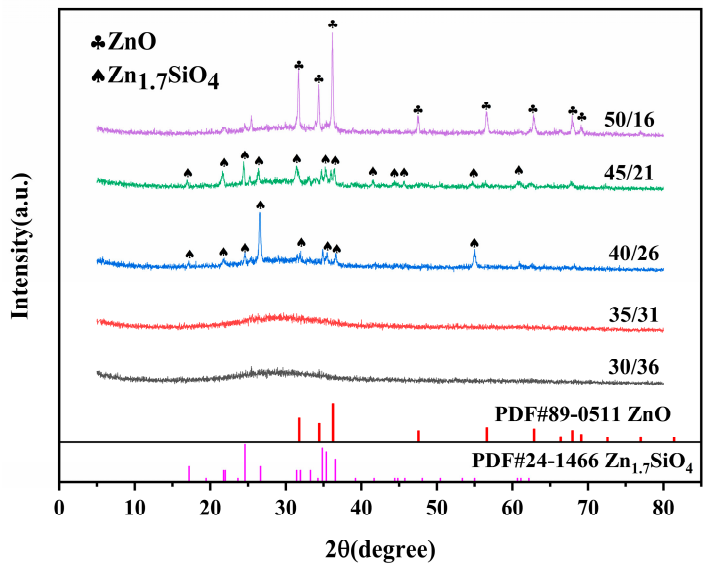

Figure 5. XRD patterns of glass inks without TiO_2 after sintering by varying the ZnO/SiO_2 ratios.

XRD patterns of the photovoltaic glass ink coatings after sintering is shown in Figure 6. All the samples are composed of TiO_2 (PDF#76-1938) and Zn_2TiO_4 crystals (PDF#73-0578). The diffraction peak at 2θ of 29.86°, 35.17°, 42.74°, 53.00°, 56.50°, and 62.04° correspond to the (2 2 0), (3 1 1), (4 0 0), (4 2 2), (5 1 1), and (4 4 0) faces of Zn_2TiO_4 crystals, respectively. With the increase in ZnO/SiO_2 (i.e., ZnO increases and SiO_2 content decreases), the diffraction peaks of Zn_2TiO_4 crystals become sharp, which indicates that the crystallinity of the samples increases. It can be seen that when TiO_2 is added to the sample, Zn_2TiO_4 and TiO_2 exist in the samples, which is obviously different from ZnO and $Zn_{1.7}SiO_4$ crystals without TiO_2 in Figure 5 due to the large amount of TiO_2 (rutile) in the ink inducing the precipitation of ZnO crystals from the glass melt [20]. According to the principle of dot-matrix matching and the condition of directional adsorption of substances [21,22], the smaller difference (not more than ±15%) in lattice constants between the crystalline phase and the nucleating agent embryo, the interfacial tension between the two phases is smaller, and thus the interfacial energy consumption of the new precipitated phase is smaller, which leads to the better precipitation. Compared with the lattice constants of TiO_2 [23] (PDF#76-1938 $a_0 = 4.593$, $b_0 = 4.593$, $c_0 = 2.95$), ZnO [24] (PDF#89-0511 $a_1 = 3.351$, $b_1 = 3.351$, $c_1 = 5.226$) belongs to a hexagonal close-packed structure, which is $c_1 \approx 2c_0$. The difference between the two crystalline phases on the c-axis is calculated to be about −11.4%, which is less than 15%. The lattice constants of $Zn_{1.7}SiO_4$ (PDF#24-1466 $a_2 = 5.069$, $b_2 = 10.292$, $c_2 = 6.677$): $b_2 \approx 2b_0$, the difference between the two crystalline phases on the b-axis is about 12.04% less than 15%. It is obvious that the difference in lattice constants between ZnO (−11.4%) is smaller than that of $Zn_{1.7}SiO_4$ (12.04%). Therefore, Zn_2TiO_4 crystals are more available for the sample by adding TiO_2, which reacts with ZnO to form Zn_2TiO_4 according to Equation (1) [25]:

$$TiO_2\ (S) + ZnO\ (S) \rightarrow Zn_2TiO_4\ (S) \quad (1)$$

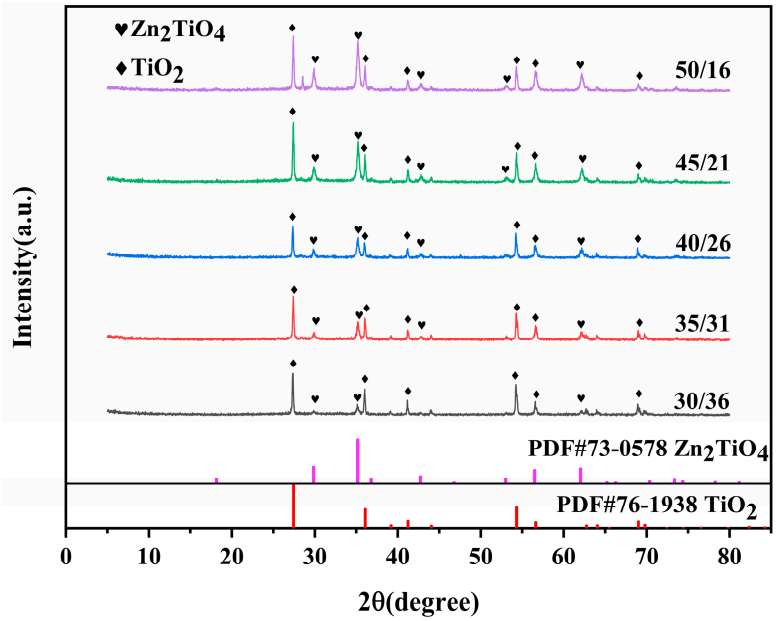

Figure 6. XRD patterns of the photovoltaic glass ink coatings with TiO_2 after sintering by varying the ZnO/SiO_2 ratios.

From the thermodynamic theory, according to the equilibrium equation $\Delta G = \Delta H - T\Delta S$ [26,27], $\Delta G = -11$ KJ < 0 at T = 700 °C is calculated, which further indicates that the reaction Equation (1) can proceed positively to form Zn_2TiO_4 crystals.

3.4. SEM Analysis

Figure 7 shows SEM surface images of the photovoltaic glass ink coatings prepared with different ZnO/SiO_2 (i.e., ZnO increases and SiO_2 content decreases). It can be seen

that the Z1 (30/36) sample exhibits a lot of large pores (Figure 7a). With the increase in ZnO/SiO_2, the pores become small and decrease in the samples. It can be concluded that the increase in ZnO/SiO_2 in the glass melt is helpful for the denseness of the samples. The reason may be that the increase in ZnO/SiO_2 in the melt leads to more and more obvious crystal formation (Figure 6), which can fill some pores. In addition, ZnO can lower the melting temperature, and thus promote more glass phases [28], resulting in the photovoltaic glass ink surface becoming dense.

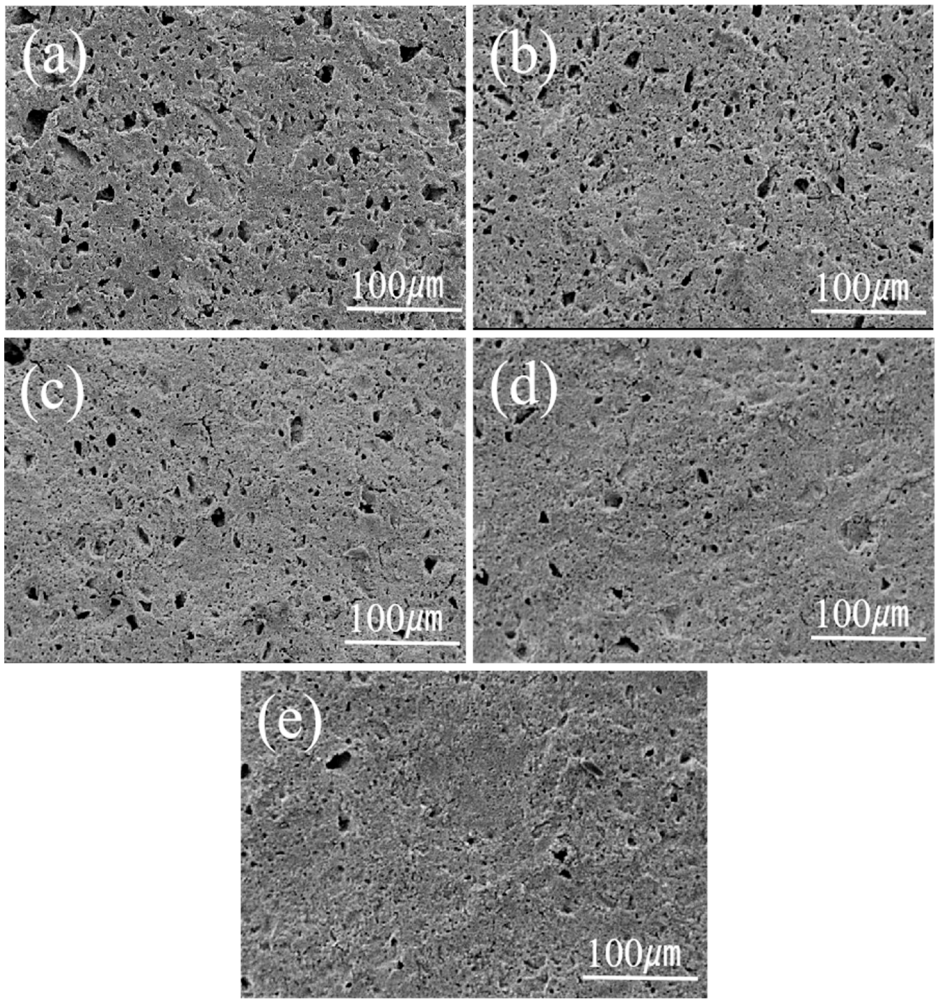

Figure 7. SEM patterns of the photovoltaic glass ink coatings after sintering by varying the ZnO/SiO_2 ratio: (**a**) 30/36, (**b**) 35/31, (**c**) 40/26, (**d**) 45/21, (**e**) 50/16.

To further analyse the microstucture of the typical samples, EDS analysis of the typical sample is shown in Figure 8. It can be seen that Zn and Ti elements are uniformly distributed in the sample. Figure 8e,f show the EDS spectra of 1 and 2 in Figure 8a, respectively. It can be clearly seen that Zn atom content has a significant increase of 9.4% and 24.6% for Zn atoms of 1 and 2 in Figure 8a, respectively. Ti content in the large particles in Figure 8e is high, which may be attributed to rutile TiO_2 (Figure 9a,b).

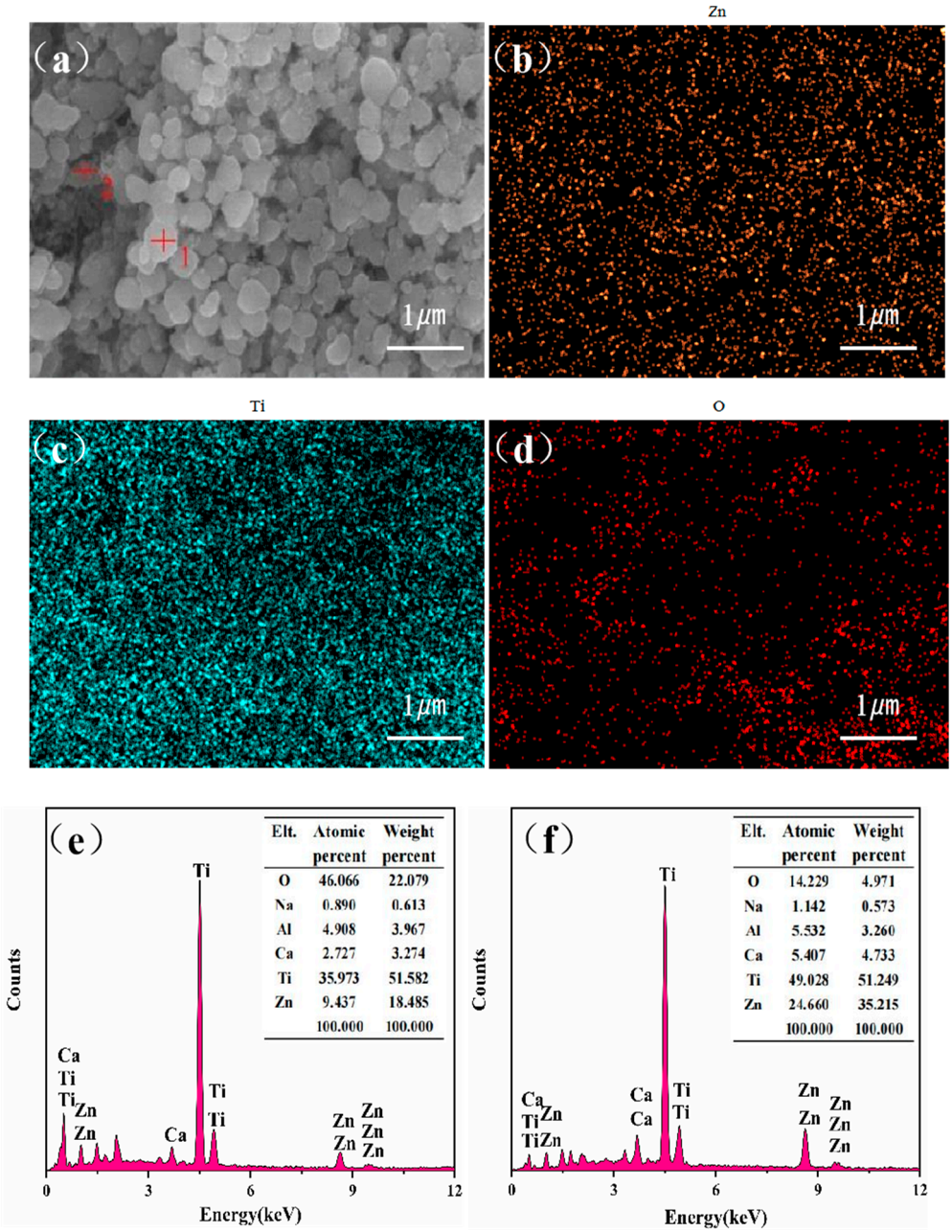

Figure 8. (**a**) FESEM images; (**b**–**d**) are elemental analyses (EDS) of Zn, Ti, and O, respectively; (**e**,**f**) EDS energy spectrum in points 1 and 2 of the typical photovoltaic glass ink coatings after sintering (40/26), respectively.

Figure 9a,b show the typical SEM images of the pure TiO_2 (rutile) samples. The sample is composed of the spherical particles with the mean sizes of 200–300 nm. It can be seen that with the increase in ZnO/SiO_2 (i.e., ZnO increases and SiO_2 content decreases), the surface of the large rutile TiO_2 particles become coarse and there are many small Zn_2TiO_4 particles adsorbed on its surface.

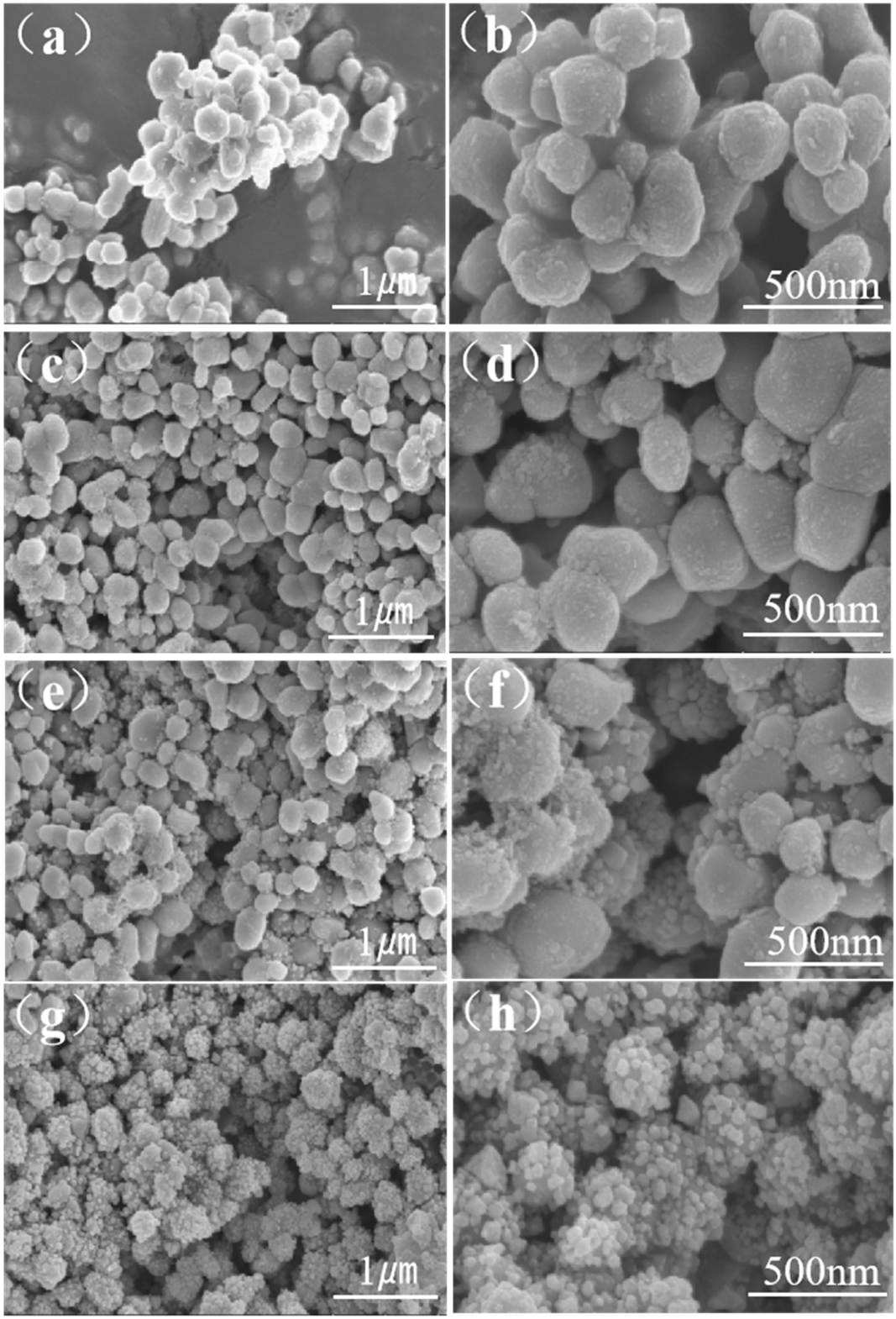

Figure 9. Typical SEM images of pure TiO_2 (**a**,**b**). After sintering (**c**–**h**), photovoltaic glass ink coatings with ratios of 30/36, 40/26, and 50/16 were prepared.

Surface roughness plays an important role in the reflectivity of coatings [29,30]. Figure 10 shows AFM images of the typical samples in the range of 10 μm and their roughness is 0.7 μm, 0.2 μm, and 0.2 μm, respectively. The surface roughness of the sample may be mainly attributed to the increase in glass phase and crystals with the increase in ZnO/SiO_2

ratio (Figures 6 and 7 and S1), which could fill more pores and make the surface of the sample flatter (Figures 7 and 9), thus decreasing the roughness of the samples.

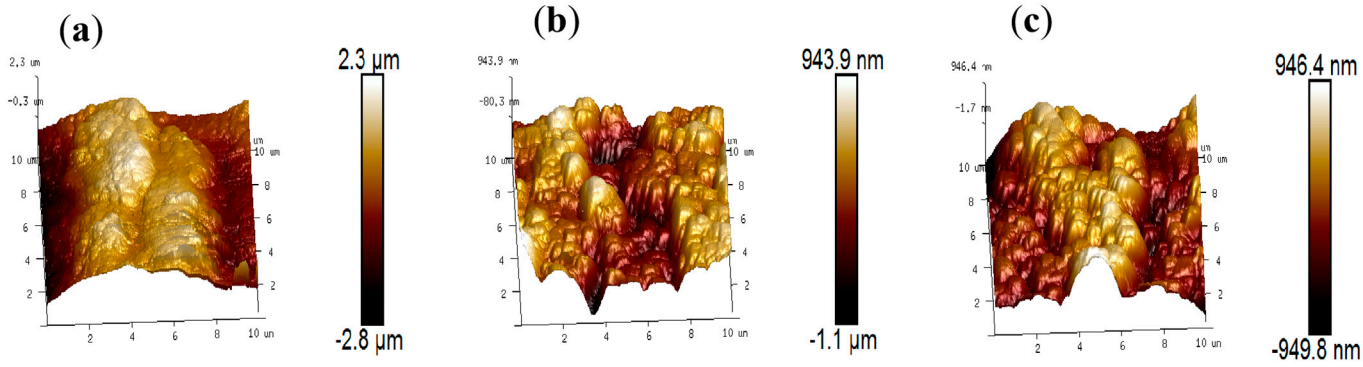

Figure 10. AFM images of the photovoltaic glass ink coatings after sintering by varying the ZnO/SiO_2 ratio: (**a**) 30/36, (**b**) 40/26, (**c**) 50/16.

3.5. Properties

Figure 11a shows the whiteness and reflectance curves of the photovoltaic glass ink coatings. It can be seen that the whiteness and reflectance of the samples firstly increased and then decreased. The samples show high diffuse reflectance in the visible band of 85.7%, 87.8%, 88.0%, 87.6%, and 86.8%, respectively. The whiteness of the samples were 85.7%, 89.2%, 89.2%, 88.3% and 88.4%, respectively. Figure 11b shows the UV-visible diffuse reflectance spectra of the typical samples. The 40/26 sample has a relatively high reflectance in the visible range. When ZnO/SiO_2 (i.e., ZnO increases and SiO_2 content decreases) is 30/36, the low reflectivity and whiteness of the sample is due to the large holes on its surface (Figure 7a), the holes could adsorb or make the light directly through the ink layer, which decreases the diffuse reflectance of the sample. With the increase in ZnO/SiO_2, many Zn_2TiO_4 crystals can fill the holes and grow on the surface and interstices of TiO_2 (Figure 9), which increases the reflective surface area and thus improves the whiteness and reflectance of the sample [9]. It is well known that the greater the refractive index of the samples in the same medium, the greater the reflectance of the sample [31]. As can be seen from the experimental results (Figures 5–9), although the 30/36 sample has a large number of pores and a small amount of Zn_2TiO_4 crystals, the surface roughness is large, and the reflection area of TiO_2 is exposed, so the reflectivity of the 30/36 sample is high. For 40/26 compared with 30/36, although more Zn_2TiO_4 crystals were grown on the surface of TiO_2 particles, the exposed reflection area of TiO_2 was still large. At the same time, more Zn_2TiO_4 crystals can be filled into the pores, which is the main factor, thus effectively improving the reflectivity of the sample. However, further increasing ZnO/SiO_2 (50/16), too many crystals grow on the surface of TiO_2 particles, thus reducing the reflective area of TiO_2. The reflectivity of the samples decreases due to the refractive index of TiO_2 greater than that of Zn_2TiO_4, keeping almost the same surface roughness. Further increasing ZnO/SiO_2, more and more crystals fill the tiny holes on the surface of the sample (Figure 7 (50/16)) and the surface roughness of the sample decreases (Figure 10), resulting in the reflectivity decrease of the sample. In addition, the average refractive index of TiO_2 (rutile) is 3.0–2.6 (400–700 nm) [32], the refractive index of Zn_2TiO_4 is 2.8–2.1 (400–700 nm) [33]. The average refractive index of TiO_2 (2.72) is greater than that of Zn_2TiO_4, and more small crystals grow on the surface of TiO_2 (Figure 9), resulting in a decrease in the surface reflection area of TiO_2, and TiO_2 is also consumed to generate Zn_2TiO_4 crystals. As a result, the whiteness and reflectivity of the sample are reduced.

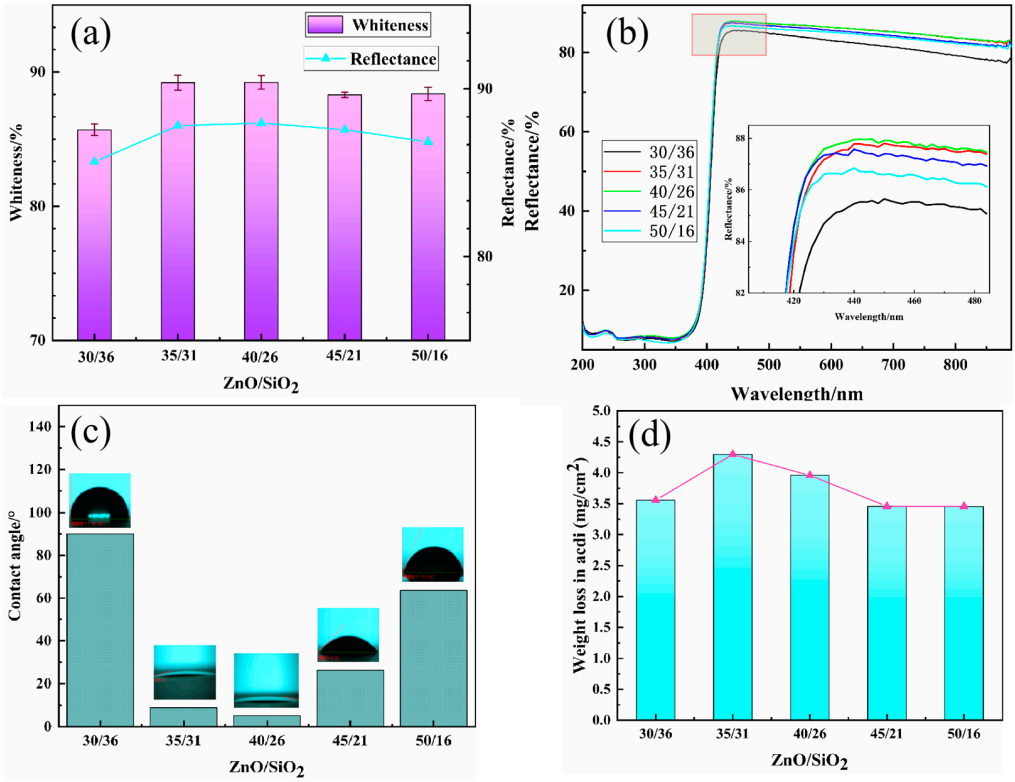

Figure 11. (**a**) The whiteness and reflectance. (**b**) UV-visible diffuse reflectance profiles of the typical samples prepared by varying the ZnO/SiO_2 ratio. (**c**) Wetting angle diagram of the photovoltaic glass ink coatings after sintering by varying the ZnO/SiO_2 ratio. (**d**) Acid resistance curves of the photovoltaic glass ink coatings after sintering.

As is well known, the surface roughness and crystallisation behavior of the coatings are indirectly related to the wetting behaviour. To further characterise the surface and crystallisation behavior, the wetting angles of the sample with different ZnO/SiO_2 ratio are characterised by the wetting angle test (Figure 11c). With the further increase in ZnO/SiO_2 ratio, the wetting angle of the sample first decreases and then increases. When the ZnO/SiO_2 ratio is 35/31 and 40/26, respectively, the wetting angle of the samples reaches the super-hydrophilic nature (about 9.0° and 5.2°), which is due to the super-hydrophilic TiO_2 [34] (Figure 6). Further increasing ZnO/SiO_2 ratio to more than 45/21, the wetting angle of the sample increases, which is due to more glass phase and crystal growth on the surface of TiO_2, and the contact area between TiO_2 and water is reduced (Figures 7–9).

Figure 11d shows the acid resistance curves of the samples prepared with different ZnO/SiO_2 (i.e., ZnO increases and SiO_2 content decreases). The mass loss of the samples in the acid solution increases and then decreases with the increase in ZnO/SiO_2. It is well known that the higher SiO_2 content in the glass, the better the acid resistance, but at the same time, the melting temperature of SiO_2 is very high, so it is necessary to control SiO_2 content appropriately [35]. The mass loss increase of the samples should be caused by the decrease in SiO_2 content, and the mass loss decrease may be due to the precipitation of more Zn_2TiO_4 nanocrystals grains (Figures 6 and 9) and the densification in the coatings, which prevent the contact between the acid solution and the glassy phase.

It can be seen from Table 1 that the sample in our study has relatively higher reflectivity and acid resistance than those in the reported literature, which is further applied for the photovoltaic modules.

Table 1. Comparison of the performance in this study with the literature.

Type of Low-Melting Glass	Scope of Application	Filler	Firing Process	Crystal	Max Reflectance	Acid Resistance	Ref.
ZnO-B_2O_3-SiO_2	Photovoltaic back glass	TiO_2	700 °C 5 min	Zn_2TiO_4	88.00%	3.9 mg/cm^2	This work
Bi_2O_3-ZnO-B_2O_3-SiO_2	Photovoltaic back glass	TiO_2	720 °C 6 min	$Bi_2Ti_2O_7$	86.18%	-	[9]
ZnO-B_2O_3-SiO_2	Photovoltaic back glass	TiO_2	600–760 °C 6 min	$ZnTiO_3$	85.89%	-	[7]
R_2O-Bi_2O_3-B_2O_3-SiO_2	Automobile glass	$CuCr_2O_4$	720 °C 210 s	$Bi_4Si_3O_{12}$	-	2.9×10^{-6} g·cm^{-2}·min^{-1}	[36]

4. Conclusions

Zn_2TiO_4 crystals were prepared for the first time in photovoltaic glass ink coating at the low-temperature of 700 °C for 5 min. Tg and Tp of the glass melt sample decreases with the increase in ZnO/SiO_2 ratio. Zn_2TiO_4 crystals increase and then decrease with the increase in ZnO/SiO_2 ratio. However, the acid resistance of the samples is enhanced when the ZnO/SiO_2 ratio is 40/26, the reflectivity and whiteness of the sample is 88.0% and 89.2%, and the weight loss in acid is 3.9 mg/cm^2, respectively. It can be attributed that Zn_2TiO_4 crystals filled the pores and thus increased the surface area of the reflected light, which improved the reflectivity and whiteness of the sample. However, many Zn_2TiO_4 crystals were harmful for the reflectivity and whiteness of the sample. This work provides a reference for quickly obtaining the crystals in the glass to improve the high reflectivity and acid resistance, which could be extended to other glass inks in the solar energy, sealing, automotive glass ink and other fields.

Supplementary Materials: The following supporting information can be downloaded at: https://www.mdpi.com/article/10.3390/inorganics12060169/s1, Figure S1: Thermal expansion test diagram of low-melting glass; Figure S2: Infrared absorption spectra of low-melting glass samples prepared with different ZnO/SiO_2 molar ratios.

Author Contributions: Methodology, Y.C., W.D., Q.B., T.Z., Z.C. and Y.X.; Investigation, Q.B.; Resources, Q.B. and T.Z.; Data curation, Y.C.; Writing—original draft, Y.C. and W.D.; Writing—review & editing, W.D. All authors have read and agreed to the published version of the manuscript.

Funding: We would like to express our gratitude for the financial support from Major Project of Natural Science Foundation of Jiangxi Province (No. 20232ACB204017), Jingdezhen technology bureau (No. 2021GYZD009-18 and No. 20224GY008-16) and Jiangxi Province Key R&D Program in China (No. 20202BBE53012), Graduate Innovation Fund Project of Jingdezhen Ceramic University (No. JYC202004).

Data Availability Statement: The raw data required to reproduce these findings cannot be shared at this time as the data also forms part of an ongoing study. Requests to access the datasets should be directed to the corresponding author.

Conflicts of Interest: The authors declare no conflict of interest.

References

1. Liu, J.; Mooney, H.; Hull, V.; Davis, S.J.; Gaskell, J.; Hertel, T.; Lubchenco, J.; Seto, K.C.; Gleick, P.; Kremen, C.; et al. Systems integration for global sustainability. *Science* **2015**, *347*, 1258832. [CrossRef] [PubMed]
2. Maleki, A.; Pourfayaz, F.; Hafeznia, H.; Rosen, M.A. A novel framework for optimal photovoltaic size and location in remote areas using a hybrid method: A case study of eastern Iran. *Energy Convers. Manag.* **2017**, *153*, 129–143. [CrossRef]
3. Fritts, C.E. On the fritts selenium cells and batteries. *J. Frankl. Inst.* **1885**, *119*, 221–232. [CrossRef]
4. Ramiro, I.; Marti, A. Intermediate band solar cells: Present and future. *Prog. Photovolt. Res. Appl.* **2021**, *29*, 705–713. [CrossRef]
5. Shang, A.; Li, X. Photovoltaic Devices: Opto-Electro-Thermal Physics and Modeling. *Adv. Mater.* **2017**, *29*, 1603492. [CrossRef] [PubMed]

6. Kim, N.; Lee, S.; Zhao, X.G.; Kim, D.; Oh, C.; Kang, H. Reflection and durability study of different types of backsheets and their impact on c-Si PV module performance. *Sol. Energy Mater. Sol. Cells* **2016**, *146*, 91–98. [CrossRef]
7. Zhou, J.; Jiao, J.; Luo, D.; Yang, J.; Zhan, L.; Xiong, D.; Li, H. B_2O_3-ZnO-SiO_2 low-melting glass and its application in high reflective white glass ink. *J. Non-Cryst. Solids* **2023**, *617*, 122511. [CrossRef]
8. Ponce-Alcántara, S.; Arangú, A.V.; Plaza, G.S. The importance of optical characterization of PV backsheets in improving solar module power. In Proceedings of the 8th International Photovoltaic Power Generation Conference Exhibition, Shanghai, China, 20–22 May 2014; Volume 20.
9. Jiao, J.; Yang, M.; Li, J.; Xiong, D.; Li, H. A novel high reflective glass-ceramic ink with $Bi_2Ti_2O_7$ nanocrystals used for the photovoltaic glass backplane. *J. Eur. Ceram. Soc.* **2023**, *43*, 3630–3636. [CrossRef]
10. Moghtada, A.; Shahrouzianfar, A.; Ashiri, R. Facile synthesis of $NiTiO_3$ yellow nano-pigments with enhanced solar radiation reflection efficiency by an innovative one-step method at low temperature. *Dye. Pigment.* **2017**, *139*, 388–396. [CrossRef]
11. Kang, J.; Wang, J.; Zhou, X.; Yuan, J.; Hou, Y.; Qian, S.; Li, S.; Yue, Y. Effects of alkali metal oxides on crystallization behavior and acid corrosion resistance of cordi-erite-based glass-ceramics. *J. Non-Cryst. Solids* **2018**, *481*, 184–190. [CrossRef]
12. Annapurna, K.; Dwivedi, R.N.; Kundu, P.; Buddhudu, S. Blue emission spectrum of Ce_3+: ZnO-B_2O_3-SiO_2 optical glass. *Mater. Lett.* **2004**, *58*, 787–789. [CrossRef]
13. Shen, Y.; Hou, L.; Zuo, G.; Li, F.; Meng, Y. Preparation of ZnO–B_2O_3–SiO_2: Mn_2+ optical-storage glass–ceramics with different ZnF_2 dopant by sol–gel method. *J. Sol-Gel Sci. Technol.* **2015**, *73*, 192–198. [CrossRef]
14. Sridharan, S.; Blonski, R.P.; Emlemdi, H.B.; Roberts, G.J.; Joyce, I.H. Glass Enamel for Automotive Applications. U.S. Patent US6105394A, 22 August 2000.
15. Wang, M.; Fang, L.; Li, M.; Liu, Z.; Hu, Y.; Zhang, X.; Deng, W.; Dongol, R. Phase separation and crystallization of La_2O_3 doped ZnO-B_2O_3-SiO_2 glass. *J. Rare Earths* **2019**, *37*, 767–772. [CrossRef]
16. Gad-Allah, T.A.; Margha, F.H. Photoactive transparent nano-crystalline glass-ceramic for remazole red dye degradation. *Mater. Res. Bull.* **2012**, *47*, 4096–4100. [CrossRef]
17. Liu, L.; Chan, K.C.; Pang, G.K.H. High-resolution TEM study of the microstructure of $Zr_{65}Ni_{10}Cu_{7.5}Al_{7.5}Ag_{10}$ bulk metallic glass. *J. Cryst. Growth* **2004**, *265*, 642–649. [CrossRef]
18. Pelino, M.; Cantalini, C.; Veglio', F.; Plescia, P.P. Crystallization of glasses obtained by recycling goethite industrial wastes to produce glass-ceramic materials. *J. Mater. Sci.* **1994**, *29*, 2087–2094. [CrossRef]
19. Zhou, W.; Li, X.; Yao, F.; Zhang, H.; Sun, K.; Chen, F.; Xu, P.; Li, X. Chip-Based MEMS Platform for Thermogravimetric/Differential Thermal Analysis (TG/DTA) Joint Characterization of Materials. *Micromachines* **2022**, *13*, 445. [CrossRef] [PubMed]
20. Holand, W.; Beall, G.H. *Glass-Ceramic Technology*; John Wiley & Sons: Hoboken, NJ, USA, 2019.
21. Xing, J.; Song, S.; Xu, X. Preparation of gold tailings glass-ceramics. *Chin. J. Nonferrous Met.* **2001**, *11*, 1004-0609.
22. Yimam, D.; Ahmadi, M.; Kooi, B. Van der Waals epitaxy of pulsed laser deposited antimony thin films on lattice-matched and amorphous substrates. *Mater. Today Nano* **2023**, *23*, 100365. [CrossRef]
23. Tian, Y.; Ding, J.; Huang, X.; Song, K.; Lu, S.-Q.; Zheng, H.-R. Development of novel interatomic potentials for simulation of rutile TiO_2. *Phys. B Condens. Matter* **2019**, *574*, 311657. [CrossRef]
24. Colak, H.; Karaköse, E. Synthesis and structural, electrical, optical properties of Lu_3+-doped ZnO nanorods. *Mater. Sci. Semicond. Process.* **2019**, *101*, 230–237. [CrossRef]
25. Meyer, A.; Toma, F.-L.; Kunze, O.; Böhme, A.; Matthey, B.; Potthoff, A.; Kaiser, A.; Gestrich, T.; Leyens, C. Development of Suspension Feedstocks for Thermally Sprayed Zn_2TiO_4 Coatings. *J. Therm. Spray Technol.* **2023**, *32*, 502–513. [CrossRef]
26. Castellan, G.W. Photophysical Processes: Fluorescence and Phosphorescence. In *Physical Chemistry*, 3rd ed.; Addison-Wesley Publishing Company, Inc.: Reading, MA, USA, 1983; pp. 891–896.
27. Peng, X.L.; Jiang, R.; Jia, C.S.; Zhang, L.H.; Zhao, Y.L. Gibbs free energy of gaseous phosphorus dimer. *Chem. Eng. Sci.* **2018**, *190*, 122–125. [CrossRef]
28. Lee, C.S.; Matori, K.A.; Ab Aziz, S.H.; Kamari, H.M.; Ismail, I.; Zaid, M.H.M. Influence of zinc oxide on the physical, structural and optical band gap of zinc silicate glass system from waste rice husk ash. *Optik* **2017**, *136*, 129–135. [CrossRef]
29. Gao, L.; Ma, Z.; Wang, F.; Li, W. Reflectivity and laser irradiation of plasma sprayed Al coating. In Proceedings of the Third International Symposium on Laser Interaction with Matter, Nanjing, China, 2–5 November 2014; SPIE: Bellingham, DC, USA, 2015; Volume 9543, pp. 143–147.
30. Luo, X.-T.; Li, S.-P.; Li, G.-C.; Xie, Y.-C.; Zhang, H.; Huang, R.-Z.; Li, C.-J. Cold spray (CS) deposition of a durable silver coating with high infrared reflectivity for radiation energy saving in the polysilicon CVD reactor. *Surf. Coatings Technol.* **2021**, *409*, 126841. [CrossRef]
31. Jeon, J.; Lee, J.; Hwang, S.; Ahn, J.; Kim, H. Influence of refractive indices of glass matrix on the reflectance of glass composites. *Met. Mater. Int.* **2011**, *17*, 593–598. [CrossRef]
32. Möls, K.; Aarik, L.; Mändar, H.; Kasikov, A.; Niilisk, A.; Rammula, R.; Aarik, J. Influence of phase composition on optical properties of TiO_2: Dependence of refractive index and band gap on formation of TiO_2-II phase in thin films. *Opt. Mater.* **2019**, *96*, 109335. [CrossRef]
33. Li, L.; Fan, Y.; Wang, D.; Feng, G.; Xu, D. Refractive index dispersion of spinel Zn_2TiO_4 single crystal. *Cryst. Res. Technol.* **2011**, *46*, 475–479. [CrossRef]

34. Shukla, G.; Angappane, S. Highly transparent, superhydrophilic and high-temperature stable anatase phase TiO_2. *Mater. Chem. Phys.* **2023**, *301*, 127589. [CrossRef]
35. Ramachandran, B.E.; Pai, B.C.; Balasubramanian, N. Studies on the Acid Resistance of E Glass. *J. Am. Ceram. Soc.* **1980**, *63*, 1–3. [CrossRef]
36. Zhao, T.G.; Wang, W.; Liu, K.; Liu, L.; Dong, W.; Bao, Q.; Xu, H.; Zhou, J. Preparation of glass-ceramics in the R_2O-Bi_2O_3-B_2O_3-SiO_2 system applied in automobile glass ename. *Inorganics* **2023**, *11*, 166. [CrossRef]